NANO LETTERS

pubs.acs.org/NanoLett
Letter

Mechanisms of Electrical Switching of Ultrathin CoO/Pt Bilayers

Christin Schmitt, Adithya Rajan, Grischa Beneke, Aditya Kumar, Tobias Sparmann, Hendrik Meer, Beatrice Bednarz, Rafael Ramos, Miguel Angel Niño, Michael Foerster, Eiji Saitoh, and Mathias Kläui*

Cite This: *Nano Lett.* 2024, 24, 1471−1476

ABSTRACT: We study current-induced switching of the Néel vector in CoO/Pt bilayers to understand the underlying antiferromagnetic switching mechanism. Surprisingly, we find that for ultrathin CoO/Pt bilayers electrical pulses along the same path can lead to an increase or decrease of the spin Hall magnetoresistance signal, depending on the current density of the pulse. By comparing these results to XMLD-PEEM imaging of the antiferromagnetic domain structure before and after the application of current pulses, we reveal the details of the reorientation of the Néel vector in ultrathin CoO(4 nm). This allows us to understand how opposite resistance changes can result from a thermomagnetoelastic switching mechanism. Importantly, our spatially resolved imaging shows that regions where the current pulses are applied and regions further away exhibit different switched spin structures, which can be explained by a spin−orbit torque-based switching mechanism that can dominate in very thin films.

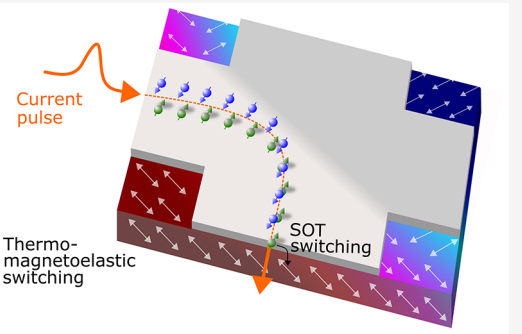

KEYWORDS: *insulating antiferromagnets, magnetization switching, spintronics, magnetic domains, spin Hall magnetoresistance*

Antiferromagnets have emerged as promising candidates for future spintronic devices,[1] offering unique properties to overcome limitations posed by current systems using ferromagnets as active elements. Their zero net magnetic moment enables higher bit packing densities and enhanced stability against external magnetic fields.[2,3] Furthermore, their internal dynamics with resonant frequencies in the THz range open up possibilities for ultrafast applications.[4] Insulating antiferromagnetic materials, with low damping enabling the transport of pure spin currents over long distances,[5,6] hold particular interest for low-power device development. However, the absence of a net magnetic moment in antiferromagnets makes efficient reading and writing of magnetic information challenging. It has been established that for insulating AFMs, electrical currents in an adjacent heavy metal layer can be used to read out the orientation of the Néel vector via the spin Hall magnetoresistance (SMR).[7,8] Electrical writing of information has been reported via current pulses which can induce a reorientation of the antiferromagnetic order, both in metallic AFMs[9−11] and bilayers of insulating AFMs and heavy metals.[12−14] The switching mechanism in the latter case is, however, being debated in terms of origin and efficiency. Some studies suggest that the switching can be driven by spin−orbit torques (SOTs).[12−17] Initially, it was, however, surprising to find current-induced switching for AFM films with tens of nanometers thickness given the interfacial nature of the SOTs. Further studies now suggest that the switching in these thick films is dominated by a thermomagnetoelastic mechanism, especially in materials with significant magnetostriction.[18−20] One can expect that for thicker films the switching is dominated by a thermomagnetoelastic switching mechanism while SOTs are expected to play a key role in thin films as the damping-like spin−orbit torque effective fields, generated by electrical current pulses in AFMs, scale with $1/d$, where d is the thickness of the AFM layer.[14] Thus, for electrical switching experiments on insulating antiferromagnetic materials, very thin CoO films are a promising choice. CoO is a collinear compensated AFM with a Néel temperature of T_N = 291 K in the bulk,[21−23] accessible with standard experimental setups. When CoO is grown on MgO(001) substrates under compressive strain (lattice mismatch 1.1%),[24,25] this yields T_N around room temperature and a 4-fold in-plane magnetic configuration with two orthogonal stable states.[20,26,27] Such a configuration is ideal for electrical switching experiments and reading the Néel vector via SMR.[8,13,28] However, to efficiently make use of the advantages of insulating AFMs in general and CoO in particular, a switching mechanism must be identified. And to facilitate this analysis, it needs to be understood if transport

Received: August 1, 2023
Revised: December 21, 2023
Accepted: December 21, 2023
Published: January 12, 2024

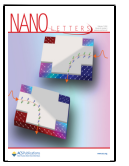

https://doi.org/10.1021/acs.nanolett.3c02890
Nano Lett. 2024, 24, 1471−1476

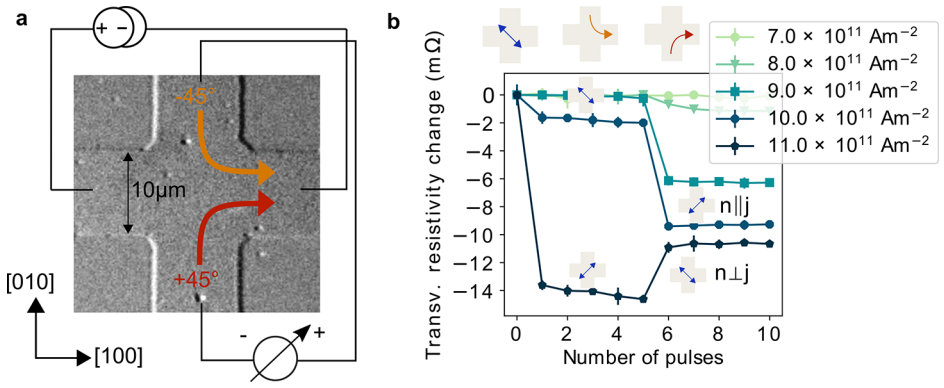

Figure 1. (a) Device and contact scheme used for the electrical measurements. The measurement current is applied along the [100] direction while the transverse voltage is read in the two arms along the [010] direction. The current pulses are in a next step applied along either the −45°- or +45°-direction with respect to the measurement current, indicated by the orange and red arrows, respectively. (b) Current density-dependent switching of the Néel vector $\boldsymbol{n}$ with respect to the current direction $\boldsymbol{j}$ in CoO(4 nm)/Pt(2 nm) thin-films showing two different switching regimes. The pulsing directions for −45°- (pulses 1−5) and +45°-pulses (pulses 6−10) are indicated by the orange and red arrows, accordingly. The blue arrows indicate the orientation of the Néel vector before and after the pulses. For low current densities $\boldsymbol{n}$ switches parallel to $\boldsymbol{j}$. For high current densities $\boldsymbol{n}$ switches perpendicular to $\boldsymbol{j}$.

measurements suffice to identify the mechanism and analyze if competing mechanisms are present simultaneously.

In this work, we investigate current-induced switching in ultrathin CoO/Pt bilayers and identify the switching mechanism by combining electrical measurements and magnetic domain imaging at different pulse current densities. Initially, we observe different switching signs in electrical SMR measurements for ultrathin CoO films. Through direct imaging, we show that the electrically observed switching of both signs can be attributed to a single thermomagnetoelastic process. However, further analysis reveals specific regions in which an additional SOT-based mechanism contributes to the switching. Our findings highlight that transport measurements alone are not sufficient to identify the switching mechanism. Instead, direct imaging of the antiferromagnetic domain structure in ultrathin samples reveals that both thermomagnetoelastic switching and SOT-switching together result in the observed current-induced spin structure changes.

To investigate the current-induced effects on the antiferromagnetic domain structure, we have grown epitaxial CoO(d)/Pt(2 nm) bilayers on MgO(001) substrates with d = 4 and 2 nm. Using Ar ion beam etching, we have patterned Hall cross structures with a channel width of 10 μm, aligning the arms of the cross parallel to the [100] and [010] sample edges (hard axes), as shown in Figure 1a. Edge pulses around the corners of the cross result in current directions $\boldsymbol{j}$ in the center of the device parallel or perpendicular to the two easy axes ([110] and [1$\bar{1}$0]). The layout allows for a reproducible switching between two orthogonal Néel vector orientations. Current pulses 1 ms long of varying current density are applied to the device. The resulting orientation of the Néel vector $\boldsymbol{n}$ is read electrically, via the transverse SMR signal, which is proportional to the in-plane Néel vector components $n_x \cdot n_y$[8] (see Supporting Information).

First, we investigate switching in a CoO(4 nm)/Pt(2 nm) film at 200 K. Before measurements, a magnetic field $\mu_0 \boldsymbol{H}_{\text{before}}$ = 12 T is applied along the [110] direction to set the Néel vector $\boldsymbol{n}$ into a defined starting state along the [1$\bar{1}$0] direction (blue double arrow in Figure 1b). Subsequently, five pulses at −45° ([1$\bar{1}$0]) and five pulses at +45° ([110]) with respect to the measurement current direction are applied. We note that transport experiments are prone to artifacts.[29−31] Therefore, we have here checked that for the current densities used, we are in a regime with no significant electromigration effects.[31] At low current densities $j_{\text{pulse}} \leq 8 \times 10^{11}$ A m^{-2} no current-induced switching is detected in the SMR signal (Figure 1b). Increasing the current density to $j_{\text{pulse}} = 9 \times 10^{11}$ A m^{-2} shows no change in the SMR signal after five pulses at −45° but a decrease in the transverse SMR signal after the first pulse along +45°, indicating a partial switching of the magnetic structure with a final state of the Néel vector $\boldsymbol{n}\|\boldsymbol{j}$ (along [110]). j_{pulse} = 10×10^{11} A m^{-2} shows a small decrease in the transverse resistivity after the first −45°-pulse, consistent with a reorientation of $\boldsymbol{n}$ (final state [110]) perpendicular to the current direction ($\boldsymbol{j}\|[1\bar{1}0]$). The SMR signal after the first +45°-pulse decreases further, indicating larger device areas switching into the [110] direction and an opposite switching sign with $\boldsymbol{n}\|\boldsymbol{j}$, as the −45°- and +45°-pulses are perpendicular to each other. Increasing the current density further to j_{pulse} = 11×10^{11} A m^{-2} results in a more pronounced effect after a −45°-pulse and a large decrease in transverse resistivity signal can be observed, indicating a reorientation of $\boldsymbol{n}\perp\boldsymbol{j}$. However, a +45°-pulse at this current density leads to an increase in the transverse SMR signal. This change in SMR indicates a rotation of parts of the device back into the original [1$\bar{1}$0] direction and thus a switching of the Néel vector final state $\boldsymbol{n}\perp\boldsymbol{j}$. Overall, we observe two different switching signs at low and high current densities, implying the presence of two electrical switching regimes with opposite Néel vector final states in ultrathin CoO(4 nm)/Pt(2 nm) bilayers. This observation suggests that different switching mechanisms dominate at different pulse current densities.

Given the scaling of the SOT strength with layer thickness, stronger SOT-induced switching is expected for thinner films. Therefore, we also investigate an ultrathin CoO(2 nm)/Pt(2 nm) sample[14] (see Supporting Information). Similar to the 4 nm sample, two distinct switching regimes can be identified in the transport measurements. At low current densities, one observes an orientation of the Néel vector final state parallel to the current direction ($\boldsymbol{n}\|\boldsymbol{j}$), while at higher current densities, a perpendicular orientation ($\boldsymbol{n}\perp\boldsymbol{j}$) is observed. Beyond that, however, no further insights into the switching mechanisms in

https://doi.org/10.1021/acs.nanolett.3c02890
Nano Lett. 2024, 24, 1471−1476

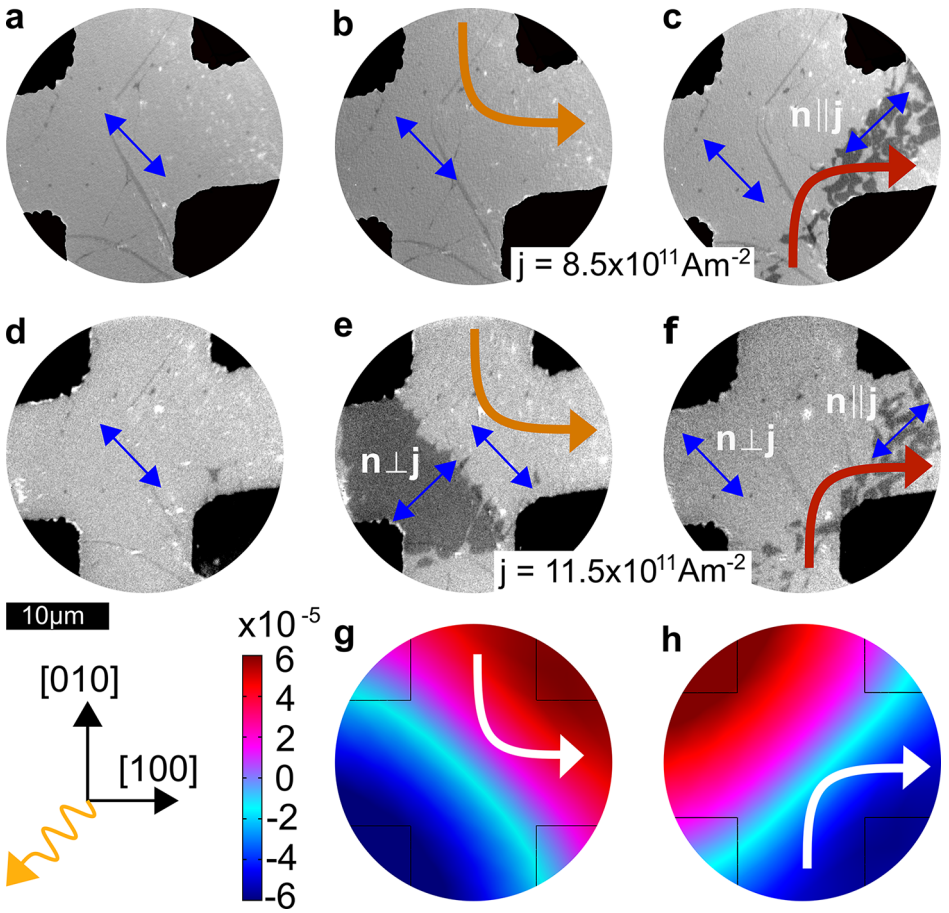

Figure 2. XMLD images of a CoO(4 nm)/Pt(2 nm) film. (a) The antiferromagnetic domain structure is in a saturated nearly monodomain state after the application of a magnetic field of 12 T at 300 K in the [110] direction. The Néel vector orientation is indicated by the blue double arrow. (b) Domain structure after the application of a −45°-pulse (orange) with j_{pulse} = 8.5 × 10^{11} A m^{-2}. (c) The application of a +45°-pulse induces some reorientation of the Néel vector with $\boldsymbol{n}\|\boldsymbol{j}$. (d) Heating the sample up above Néel temperature restores the almost monodomain state with $\boldsymbol{n}\|[1\bar{1}0]$. (e) The application of a −45°-pulse (j_{pulse} = 11.5 × 10^{11} A m^{-2}) induces a change of the antiferromagnetic domain structure. (f) Magnetic state after a +45°-pulse with j_{pulse} = 11.5 × 10^{11} A m^{-2}. (g) Strain-profile for a pulse along the −45° direction. (h) Strain-profile for a pulse along the +45° direction.

antiferromagnetic thin films are obtained from the transport study of this sample so that in the following we focus on the 4 nm thick sample.

To address the open question of whether two different mechanisms are causing the Néel vector switching in these ultrathin CoO samples, imaging of the AFM domain structure is essential, especially since transport signals can be affected by issues such as spatially varying sensitivity of the Hall cross device[32] or due to nonmagnetic contributions to the SMR signal, from e.g. electromigration effects.[31] By correlating the effect of electrical current pulses on the domain structure by imaging, we can gain insights into the mechanisms and origin of the distinct switching regimes.

By comparing the electrical signal with the changes in domain structure, we can make a direct conclusion about which of the switching signs and regimes is consistent with which proposed switching mechanism for insulating antiferromagnetic/heavy metal bilayers.[19]

To image the AFM domain structure, we use photoemission electron microscopy (PEEM) using for contrast generation the X-ray magnetic linear dichroism (XMLD) effect. We image the AFM domain structure using energy dependent XMLD-PEEM at the Co L_3 edge using two energies E_1 = 777.9 eV and E_2 = 779.0 eV. Figure 2a shows the investigated Hall bar region. Prior to the imaging, a magnetic field above the spin-flop ($\mu_0 H_{before}$ = 12 T) was applied along the [110] direction at 300 K, to set the Néel order in the same starting state as in the transport measurements with $\boldsymbol{n}\|[1\bar{1}0]$ (indicated by the blue double arrow). The sample was cooled to 220 K for the imaging and pulse application. It needs to be noted that the dark stripes in the center of the Hall cross structure are nonmagnetic and arise from surface inhomogeneities. However, since the values of the resistance in the Hall cross are comparable for all measured devices, we can conclude that the surface inhomogeneities do not affect the path of the current pulses. When applying a −45°-pulse, indicated by the orange arrow in Figure 2b, with j_{pulse} = 8.5 × 10^{11} A m^{-2}, no significant change in the magnetic domain structure is observed, consistent with the low current regime in the electrical measurements, where a −45°-pulse does not lead to an observable change in transverse Hall resistivity. However, a +45°-pulse with the same current density induces a reorientation of the Néel vector in the region of the Hall cross where the current is flowing, as shown in Figure 2c. This magnetic change is consistent with a switching of $\boldsymbol{n}\|\boldsymbol{j}$, in agreement with the low current density regime in the electrical measurements. Before the next current pulses are applied, the magnetic state of the sample was brought back into the

https://doi.org/10.1021/acs.nanolett.3c02890
Nano Lett. 2024, 24, 1471−1476

approximately monodomain state with $\boldsymbol{n}\|[1\bar{1}0]$ by heating it in situ above its Néel temperature. The subsequent application of a single pulse with $j_{\mathrm{pulse}} = 11.5 \times 10^{11}$ A m^{-2} along the −45° direction induces a change of the AFM domain structure in the arms opposite to those to which the current pulse is applied. Figure 2e shows the resulting magnetic state. The Néel vector in the switched region is oriented perpendicular to the current direction in the center of the device ($\boldsymbol{n}\perp\boldsymbol{j}$). This is in line with the sign of the switching observed in the high current density regime in the electrical measurements. A pulse with equal current density but a perpendicular direction (+45°), as shown in Figure 2f, erases parts of the previously nucleated domain structure and generates a magnetic state similar to that created when applying a smaller current density. In this case, however, the switching sign cannot be uniquely determined. In the arms of the cross opposite where the current pulse was applied, the final state of the Néel vector is $\boldsymbol{n}\perp\boldsymbol{j}$, consistent with the observations in the electrical measurements. On the other hand, in the arms where the current pulse was applied the final state is $\boldsymbol{n}\|\boldsymbol{j}$. Thus, the microscopic measurements reveal that different switching behaviors can be observed in different parts of the sample and that there are also differences depending on the current density. To infer the switching mechanism, we compare the XMLD-PEEM images with the predicted switching sign for SOTs in CoO and with the difference in strain distribution resulting from the current-induced heat, which we simulated with COMSOL. For the simulations in Figure 2g,h we plot the difference between the strain along the two easy axes $\epsilon[1\bar{1}0] - \epsilon[110]$. A positive strain difference (red) indicates a larger expansion of the CoO along $[1\bar{1}0]$ compared to [110], while a negative strain difference (blue) indicates larger strain along the orthogonal direction. The strain is caused by the expansion of the CoO lattice due to the applied current in the Pt, leading to inhomogeneous Joule heating and, thus, inhomogeneous expansion. Figure 2g,h shows the resulting strain-distributions for the pulses along the −45° and +45° directions, respectively. Comparing these strain-profiles with the XMLD-PEEM images in the low current-density regime indicates that after a −45°-pulse (Figure 2b), no switching is observed. In the region close to the applied current pulse, with sufficient heat and strain present, the Néel vector is already oriented along the [110] direction, the axis along which a stronger expansion of CoO is observed (red). In the arms opposite where the current pulse is applied, the strain is in the orthogonal direction, which could lead to a reorientation of the Néel vector. However, this is not observed, suggesting that the heat in this area may not be sufficient to trigger a switching of the Néel vector.[19] For a +45°-pulse, on the other hand, the region with stronger expansion of the CoO along $[1\bar{1}0]$ (blue) is in the arms of the cross where the current pulse is applied, and the heating is stronger. Here, a switching of the Néel vector can be observed.

The observed behavior in the low current-density regime is consistent with a thermomagnetoelastic switching mechanism. Checking the high current-density regime, we find that the changes in the Néel vector also align with a thermomagnetoelastic switching mechanism. Specifically, for the −45°-pulse there is a reorientation of the Néel vector in the arms opposite to where the current pulse is applied, which can be attributed to increased heating in that region (Figure 2e). For the +45°-pulse the resulting domain structure in the arms where the current pulse is applied switches into the $[1\bar{1}0]$ direction, consistent with the strain in the $[1\bar{1}0]$ direction, while in the opposite part, it switches back into the [110] direction, following the strain in the [110] direction (red). So this shows that the transport signals can be difficult to interpret if not complemented by direct imaging.

Most importantly, not all of the observed changes in the domain structure can be solely attributed to the thermomagnetoelastic switching mechanism. The domain structure for +45°-pulses, where the change in the Néel vector occurs in regions where the current pulses are applied, is different from that for −45°-pulses, where the change occurs in the opposite arms. For +45°-pulses, the resulting domain structure appears less homogeneous and requires a different explanation. This observation indicates the presence of different switching mechanisms. To investigate the potential presence of an SOT-based mechanism in the arms where the pulses are applied, we compare the experimentally observed switching sign with the theoretical predictions for the SOT-based switching mechanism in CoO. SOTs in AFMs are predicted to be caused by the spin accumulation at the AFM/HM interface, induced by the SHE in the HM.[13] The corresponding torques create staggered fields which remove the degeneracy between the two orthogonal easy axes, resulting in a current-induced energy term, which competes with the magnetic anisotropy.[14] In order to minimize this contribution the predicted final state of switching in CoO is $\boldsymbol{n}\|\boldsymbol{j}$.[20] For the −45°-pulses we do not observe switching at the locations of the current pulse, in agreement with an SOT switching mechanism since the Néel vector orientation is already parallel to the current direction in the center of the Hall cross. However, for +45°-pulses, we observe a switching of $\boldsymbol{n}\|\boldsymbol{j}$, in line with what is expected from an SOT-based switching mechanism. As a result, we conclude that switching in ultrathin AFM films is governed by a combination of two mechanisms: a thermomagnetoelastic switching mechanism and an SOT-based mechanism. The SOT mechanism occurs in the areas where the current pulse is applied, while the thermomagnetoelastic mechanism dominates in regions without current flow, where inhomogeneous strain distributions persist and sufficient heating facilitates the process. In the Supporting Information we provide further experimental data on the current-induced switching for the case where the starting state of the Néel vector is perpendicular to the here studied case. For a more quantitative understanding, one would require a systematic analysis of different current flow geometries, current amplitudes, and temperatures, which goes beyond the scope of this current work. For thinner samples in particular, one would expect a more pronounced effect of the SOT mechanism.

In conclusion, we have investigated current-induced switching of the Néel vector in ultrathin CoO/Pt bilayers and revealed the interplay of different switching mechanisms. In transport measurements, we find that electrical pulses along the same current path can show opposite sign for the switching-induced change of the SMR signal, depending on the current density. However, by comparing these results with the XMLD-PEEM imaging of the domain structure, we demonstrate that the current-induced switching leading to the different sign of the SMR can be explained by the action of a single heat-assisted thermomagnetoelastic switching mechanism at all current densities. This highlights the importance of magnetic imaging to reveal the full changes in the antiferromagnetic domain structure since electrical data themselves can be misleading. Most importantly, we identify

https://doi.org/10.1021/acs.nanolett.3c02890
Nano Lett. 2024, 24, 1471−1476

the presence of an SOT-based mechanism, which explains the differences in domain structure between the regions where the current pulse is applied and those opposite to it. It is expected that such an SOT-based mechanism becomes most relevant for thinner films, compared to previous reports of tens of nanometer thick films where only thermomagnetoelastic switching mechanisms were identified. These findings are key as they demonstrate the interplay of the different switching mechanisms and thus motivate further research into thinner films, offering promising opportunities for utilizing AFMs in applications where electrical reading and efficient writing through SOTs is key.

■ ASSOCIATED CONTENT

Supporting Information

The Supporting Information is available free of charge at https://pubs.acs.org/doi/10.1021/acs.nanolett.3c02890.

Growth procedure and structural characterization, SMR readout mechanism, Electrical switching of MgO(001)//CoO(2 nm)/Pt(2 nm) bilayers and competing switching mechanisms (PDF)

■ AUTHOR INFORMATION

Corresponding Author

Mathias Kläui − *Institute of Physics, Johannes Gutenberg University Mainz, 55099 Mainz, Germany; Graduate School of Excellence Materials Science in Mainz, 55128 Mainz, Germany;* orcid.org/0000-0002-4848-2569; Email: klaeui@uni-mainz.de

Authors

Christin Schmitt − *Institute of Physics, Johannes Gutenberg University Mainz, 55099 Mainz, Germany;* orcid.org/0000-0002-5340-2826

Adithya Rajan − *Institute of Physics, Johannes Gutenberg University Mainz, 55099 Mainz, Germany*

Grischa Beneke − *Institute of Physics, Johannes Gutenberg University Mainz, 55099 Mainz, Germany*

Aditya Kumar − *Institute of Physics, Johannes Gutenberg University Mainz, 55099 Mainz, Germany*

Tobias Sparmann − *Institute of Physics, Johannes Gutenberg University Mainz, 55099 Mainz, Germany*

Hendrik Meer − *Institute of Physics, Johannes Gutenberg University Mainz, 55099 Mainz, Germany;* orcid.org/0000-0003-4727-1150

Beatrice Bednarz − *Institute of Physics, Johannes Gutenberg University Mainz, 55099 Mainz, Germany*

Rafael Ramos − *WPI-Advanced Institute for Materials Research, Tohoku University, Sendai 980-8577, Japan;* Present Address: Centro Singular de Investigación en Química Biolóxica e Materiais Moleculares (CiQUS), Departamento de Química-Física, Universidade de Santiago de Compostela, Santiago de Compostela 15782, Spain

Miguel Angel Niño − *ALBA Synchrotron Light Facility, 08290 Cerdanyola del Valles (Barcelona), Spain;* orcid.org/0000-0003-3692-147X

Michael Foerster − *ALBA Synchrotron Light Facility, 08290 Cerdanyola del Valles (Barcelona), Spain*

Eiji Saitoh − *WPI-Advanced Institute for Materials Research, Institute for Materials Research, and Center for Spintronics Research Network, Tohoku University, Sendai 980-8577, Japan; The Institute of AI and Beyond, The University of Tokyo, Tokyo 113-8656, Japan; Department of Applied Physics, The University of Tokyo, Tokyo 113-8656, Japan*

Complete contact information is available at: https://pubs.acs.org/10.1021/acs.nanolett.3c02890

Author Contributions

M.K. proposed and supervised the project. C.S. performed the electrical measurements. The XMLD-PEEM measurements were performed by A.R., G.B., A.K., and T.S. with the help and supervision of M.F. and M.A.N. The experimental data was analyzed by C.S. under the supervision of M.K. C.S. performed the strain simulations with COMSOL supported by H.M. The devices were designed by C.S. and fabricated by C.S., A.R., and B.B. The antiferromagnetic thin films were grown by A.R. and R.R. with inputs from C.S. and supervised by E.S. C.S. wrote the paper with M.K. All authors commented on the manuscript.

Notes

COMSOL and COMSOL Multiphysics are registered trademarks of COMSOL AB.

The authors declare no competing financial interest.

■ ACKNOWLEDGMENTS

Experiments were performed at the CIRCE beamline at ALBA Synchrotron with the collaboration of ALBA staff. M.K. acknowledges support from the Graduate School of Excellence Materials Science in Mainz (MAINZ) DFG 266, the DAAD (Spintronics network, Project No. 57334897). We acknowledge that this work is funded by the Deutsche Forschungsgemeinschaft (DFG, German Research Foundation)—TRR 173-268565370 (Projects A01 and B02). This project has received funding from the European Union's Horizon 2020 research and innovation programme under Grant Agreement No. 863155 (s-Nebula). A.R. and B.B. acknowledge funding from the European Union's Horizon 2020 research and innovation programme under the Marie Skłodowska-Curie Grant Agreement No. 860060 (ITN MagnEFi). This work is also supported by ERATO "Spin Quantum Rectification Project" (Grant No. JPMJER1402) and the Grant-in-Aid for Scientific Research on Innovative Area, "Nano Spin Conversion Science" (Grant No. JP26103005), Grant-in-Aid for Scientific Research (S) (Grant No. JP19H05600), Grant-in-Aid for Scientific Research (C) (Grant No. JP20K05297) from JSPS KAKENHI. R.R. also acknowledges support from the Grant RYC 2019-026915-I and the Project TED2021-130930B-I00 funded by the MCIN/AEI/10.13039/501100011033 and by the ESF investing in your future and the European Union NextGenerationEU/PRTR, the Xunta de Galicia (ED431F 2022/04, ED431B 2021/013, Centro Singular de Investigación de Galicia Accreditation 2019-2022, ED431G 2019/03) and the European Union (European Regional Development Fund - ERDF).

■ REFERENCES

(1) Baltz, V.; Manchon, A.; Tsoi, M.; Moriyama, T.; Ono, T.; Tserkovnyak, Y. Antiferromagnetic spintronics. *Rev. Mod. Phys.* **2018**, *90*, 015005.

(2) Meer, H.; Gomonay, O.; Wittmann, A.; Kläui, M. Antiferromagnetic insulatronics: Spintronics in insulating 3d metal oxides with antiferromagnetic coupling. *Appl. Phys. Lett.* **2023**, *122*, 080502.

(3) Loth, S.; Baumann, S.; Lutz, C. P.; Eigler, D.; Heinrich, A. J. Bistability in atomic-scale antiferromagnets. *Science* **2012**, *335*, 196−199.
(4) Kampfrath, T.; Sell, A.; Klatt, G.; Pashkin, A.; Mährlein, S.; Dekorsy, T.; Wolf, M.; Fiebig, M.; Leitenstorfer, A.; Huber, R. Coherent terahertz control of antiferromagnetic spin waves. *Nat. Photonics* **2011**, *5*, 31−34.
(5) Lebrun, R.; Ross, A.; Bender, S.; Qaiumzadeh, A.; Baldrati, L.; Cramer, J.; Brataas, A.; Duine, R.; Kläui, M. Tunable long-distance spin transport in a crystalline antiferromagnetic iron oxide. *Nature* **2018**, *561*, 222−225.
(6) Das, S.; et al. Anisotropic long-range spin transport in canted antiferromagnetic orthoferrite $YFeO_3$. *Nat. Commun.* **2022**, *13*, 6140.
(7) Hoogeboom, G. R.; Aqeel, A.; Kuschel, T.; Palstra, T. T.; van Wees, B. J. Negative spin Hall magnetoresistance of Pt on the bulk easy-plane antiferromagnet NiO. *Appl. Phys. Lett.* **2017**, *111*, 052409.
(8) Baldrati, L.; Ross, A.; Niizeki, T.; Schneider, C.; Ramos, R.; Cramer, J.; Gomonay, O.; Filianina, M.; Savchenko, T.; Heinze, D.; et al. Full angular dependence of the spin Hall and ordinary magnetoresistance in epitaxial antiferromagnetic NiO (001)/Pt thin films. *Phys. Rev. B* **2018**, *98*, 024422.
(9) Wadley, P.; Howells, B.; Železnỳ, J.; Andrews, C.; Hills, V.; Campion, R. P.; Novák, V.; Olejník, K.; Maccherozzi, F.; Dhesi, S.; et al. Electrical switching of an antiferromagnet. *Science* **2016**, *351*, 587−590.
(10) Bodnar, S. Y.; Šmejkal, L.; Turek, I.; Jungwirth, T.; Gomonay, O.; Sinova, J.; Sapozhnik, A.; Elmers, H.-J.; Kläui, M.; Jourdan, M. Writing and reading antiferromagnetic Mn_2Au by Néel spin-orbit torques and large anisotropic magnetoresistance. *Nat. Commun.* **2018**, *9*, 348.
(11) Reimers, S.; Lytvynenko, Y.; Niu, Y.; Golias, E.; Sarpi, B.; Veiga, L.; Denneulin, T.; Kovacs, A.; Dunin-Borkowski, R.; Bläßer, J.; et al. Current-driven writing process in antiferromagnetic Mn2Au for memory applications. *Nat. Commun.* **2023**, *14*, 1861.
(12) Moriyama, T.; Oda, K.; Ohkochi, T.; Kimata, M.; Ono, T. Spin torque control of antiferromagnetic moments in NiO. *Sci. Rep.* **2018**, *8*, 14167.
(13) Chen, X.; Zarzuela, R.; Zhang, J.; Song, C.; Zhou, X.; Shi, G.; Li, F.; Zhou, H.; Jiang, W.; Pan, F.; et al. Antidamping-torque-induced switching in biaxial antiferromagnetic insulators. *Phys. Rev. Lett.* **2018**, *120*, 207204.
(14) Baldrati, L.; Gomonay, O.; Ross, A.; Filianina, M.; Lebrun, R.; Ramos, R.; Leveille, C.; Fuhrmann, F.; Forrest, T.; Maccherozzi, F.; et al. Mechanism of Néel order switching in antiferromagnetic thin films revealed by magnetotransport and direct imaging. *Phys. Rev. Lett.* **2019**, *123*, 177201.
(15) Gray, I.; Moriyama, T.; Sivadas, N.; Stiehl, G. M.; Heron, J. T.; Need, R.; Kirby, B. J.; Low, D. H.; Nowack, K. C.; Schlom, D. G.; et al. Spin Seebeck imaging of spin-torque switching in antiferromagnetic Pt/NiO heterostructures. *Physical Review X* **2019**, *9*, 041016.
(16) Cheng, Y.; Yu, S.; Zhu, M.; Hwang, J.; Yang, F. Electrical Switching of Tristate Antiferromagnetic Néel Order in $\alpha - Fe_2O_3$ Epitaxial Films. *Phys. Rev. Lett.* **2020**, *124*, 027202.
(17) Zhang, P.; Chou, C.-T.; Yun, H.; McGoldrick, B. C.; Hou, J. T.; Mkhoyan, K. A.; Liu, L. Control of Néel Vector with Spin-Orbit Torques in an Antiferromagnetic Insulator with Tilted Easy Plane. *Phys. Rev. Lett.* **2022**, *129*, 017203.
(18) Zhang, P.; Finley, J.; Safi, T.; Liu, L. Quantitative study on current-induced effect in an antiferromagnet insulator/Pt bilayer film. *Phys. Rev. Lett.* **2019**, *123*, 247206.
(19) Meer, H.; Schreiber, F.; Schmitt, C.; Ramos, R.; Saitoh, E.; Gomonay, O.; Sinova, J.; Baldrati, L.; Kläui, M. Direct imaging of current-induced antiferromagnetic switching revealing a pure thermomagnetoelastic switching mechanism in NiO. *Nano Lett.* **2021**, *21*, 114−119.
(20) Baldrati, L.; Schmitt, C.; Gomonay, O.; Lebrun, R.; Ramos, R.; Saitoh, E.; Sinova, J.; Kläui, M. Efficient spin torques in antiferromagnetic CoO/Pt quantified by comparing field-and current-induced switching. *Phys. Rev. Lett.* **2020**, *125*, 077201.
(21) Roth, W. Magnetic structures of MnO, FeO, CoO, and NiO. *Phys. Rev.* **1958**, *110*, 1333.
(22) Uchida, E.; Fukuoka, N.; Kondoh, H.; Takeda, T.; Nakazumi, Y.; Nagamiya, T. Magnetic anisotropy measurements of CoO single crystal. *J. Phys. Soc. Jpn.* **1964**, *19*, 2088−2095.
(23) Saito, S.; Nakahigashi, K.; Shimomura, Y. X-ray diffraction study on CoO. *J. Phys. Soc. Jpn.* **1966**, *21*, 850−860.
(24) Csiszar, S.; Haverkort, M.; Hu, Z.; Tanaka, A.; Hsieh, H.; Lin, H.-J.; Chen, C.; Hibma, T.; Tjeng, L. Controlling orbital moment and spin orientation in CoO layers by strain. *Phys. Rev. Lett.* **2005**, *95*, 187205.
(25) Zhu, J.; Li, Q.; Li, J.; Ding, Z.; Liang, J.; Xiao, X.; Luo, Y.; Hua, C.; Lin, H.-J.; Pi, T.; et al. Antiferromagnetic spin reorientation transition in epitaxial NiO/CoO/MgO (001) systems. *Phys. Rev. B* **2014**, *90*, 054403.
(26) Cao, W.; Li, J.; Chen, G.; Zhu, J.; Hu, C.; Wu, Y. Temperature-dependent magnetic anisotropies in epitaxial Fe/CoO/MgO (001) system studied by the planar Hall effect. *Appl. Phys. Lett.* **2011**, *98*, 262506.
(27) Grzybowski, M.; Schippers, C.; Gomonay, O.; Rubi, K.; Bal, M.; Zeitler, U.; Kozioł- Rachwał, A.; Szpytma, M.; Janus, W.; Kurowska, B.; et al. Antiferromagnetic hysteresis above the spin-flop field. *Phys. Rev. B* **2023**, *107*, L060403.
(28) Nakayama, H.; Althammer, M.; Chen, Y.-T.; Uchida, K.-i.; Kajiwara, Y.; Kikuchi, D.; Ohtani, T.; Geprägs, S.; Opel, M.; Takahashi, S.; et al. Spin Hall magnetoresistance induced by a nonequilibrium proximity effect. *Phys. Rev. Lett.* **2013**, *110*, 206601.
(29) Churikova, A.; Bono, D.; Neltner, B.; Wittmann, A.; Scipioni, L.; Shepard, A.; Newhouse-Illige, T.; Greer, J.; Beach, G. Non-magnetic origin of spin Hall magnetoresistance-like signals in Pt films and epitaxial NiO/Pt bilayers. *Appl. Phys. Lett.* **2020**, *116*, 022410.
(30) Matalla-Wagner, T.; Schmalhorst, J.-M.; Reiss, G.; Tamura, N.; Meinert, M. Resistive contribution in electrical-switching experiments with antiferromagnets. *Physical Review Research* **2020**, *2*, 033077.
(31) Schreiber, F.; Baldrati, L.; Schmitt, C.; Ramos, R.; Saitoh, E.; Lebrun, R.; Kläui, M. Concurrent magneto-optical imaging and magneto-transport readout of electrical switching of insulating antiferromagnetic thin films. *Appl. Phys. Lett.* **2020**, *117*, 082401.
(32) Schreiber, F.; Meer, H.; Schmitt, C.; Ramos, R.; Saitoh, E.; Baldrati, L.; Kläui, M. Magnetic sensitivity distribution of Hall devices in antiferromagnetic switching experiments. *Physical Review Applied* **2021**, *16*, 064023.

https://doi.org/10.1021/acs.nanolett.3c02890
Nano Lett. 2024, 24, 1471−1476